JOURNAL OF GEOPHYSICAL RESEARCH, VOL. 106, NO. A12, PAGES 29,133–29,152, DECEMBER 1, 2001

Measurement of the latitudinal distributions of total electron content during equatorial spread *F* events

C. E. Valladares,[1] S. Basu,[2] K. Groves,[2] M. P. Hagan,[1] D. Hysell,[3] A. J. Mazzella Jr.,[4] and R. E. Sheehan[1]

Abstract. We have constructed latitudinal profiles of the total electron content (TEC) using measurements from six GPS receivers conducted during 1998. The TEC profiles have been divided into two groups: One corresponds to days when plumes or equatorial spread *F* (ESF) develops, and the second group portrays days of no–ESF condition. The presence/absence of ESF is based on the signature of the coherent echoes measured by the Jicamarca Unattended Long–Term Investigation (JULIA) radar and records of scintillations from two sites spaced in latitude. One scintillation station is located near the magnetic equator (Ancon) and the other 12° southward (Antofagasta). The TEC profiles display the typical day-to-day and seasonal variability seen at low latitudes. During the equinoxes, we observed quite often the crests of the anomaly located between 12° and 20° away from the magnetic equator and a trough in–between. The monthly distribution of the appearance of the anomaly and the local time of their appearance are in very good agreement with the reported variability of the upward vertical drifts and the current theory of the equatorial fountain effect. During the equinoxes and the December solstice, the TEC anomaly is observed almost every day, sometimes when there is no ESF activity. Nevertheless, fine inspection of the TEC latitudinal profiles suggests the existence of a close relationship between the temporal evolution of the TEC profiles near sunset and the onset of ESF. We have examined the TEC latitudinal distributions in two different ways. First, we calculated time difference profiles using the distributions corresponding to 1800 and 2000 LT. Second, we used a parameterization of the TEC distributions obtained at 2000 LT. The first method indicates quite drastic increases of the crest values and sharp decreases near the trough during ESF days. In contrast, during days of no ESF there exist almost uniform TEC decreases at all latitudes. The second method displays a preferred high crest/trough ratio (>2), small TEC values at the trough, and large latitudinal integrated values during ESF events.

1. Introduction

The term equatorial spread *F* (ESF) encompasses several turbulent processes and different types of plasma instabilities that grow and propagate in the nighttime equatorial ionosphere. Since the first observation of range-dispersed ionograms in the late thirties [*Booker and Wells*, 1938], until the more refined measurements of ESF using ground-based radars and satellite-borne sensors, all have indicated the turbulent and the seemingly unpredictable nature of this phenomenon. In particular, the Jicamarca radar has been instrumental in describing the altitude distribution, time evolution, scale size, vertical and zonal drift, and the magnetic aspect angle dependence of 3-m irregularities associated with ESF [*Farley et al.*, 1970; *Woodman and LaHoz* 1976; *Kudeki et al.*, 1981; *Kelley et al.*, 1986; Farley and Hysell, 1996]. A milestone in the investigation of ESF was the observation of 3-m irregularities forming altitude–elongated "plumes," which were tracers of plasma depletions or "bubbles" advecting from the lower altitudes of the *F* layer and quite often intruding into the topside [*Woodman and LaHoz*, 1976]. These authors suggested that the time evolution of the radar plumes followed the evolution of the Rayleigh-Taylor instability (RTI). The studies undertaken by *Kelley et al.* [1976] and *McClure et al.* [1977] confirmed that the deep plasma depletions, seen at *F* region altitudes, were actually formed at the bottomside and had propagated toward higher altitudes.

In the last 25 years, further measurements of ESF using incoherent scatter radar [*Tsunoda*, 1980], probes on board satellites [*McClure et al.*, 1977; *Valladares et al.*, 1983], airglow photometers [*Mendillo et al.*, 1992], scintillation receivers [*Basu and Basu*, 1985], HF transmissions [*Jayachandran et al.*, 1993], and numerical modeling [*Ossakow et al.*, 1979; *Zalesak and Ossakow*, 1980] have indicated the general morphology of the ESF phenomenon. It

[1]Institute for Scientific Research, Boston College, Chestnut Hill, Massachusetts.
[2]Air Force Research Laboratory, Hanscom Air Force Base, Massachusetts.
[3]Department of Physics and Astronomy, Clemson University, Clemson, South Carolina.
[4]Northwest Research Associates, Bellevue, Washington.

Paper number 2000JA000426
0148-0227/01/2000JA000426$09.00

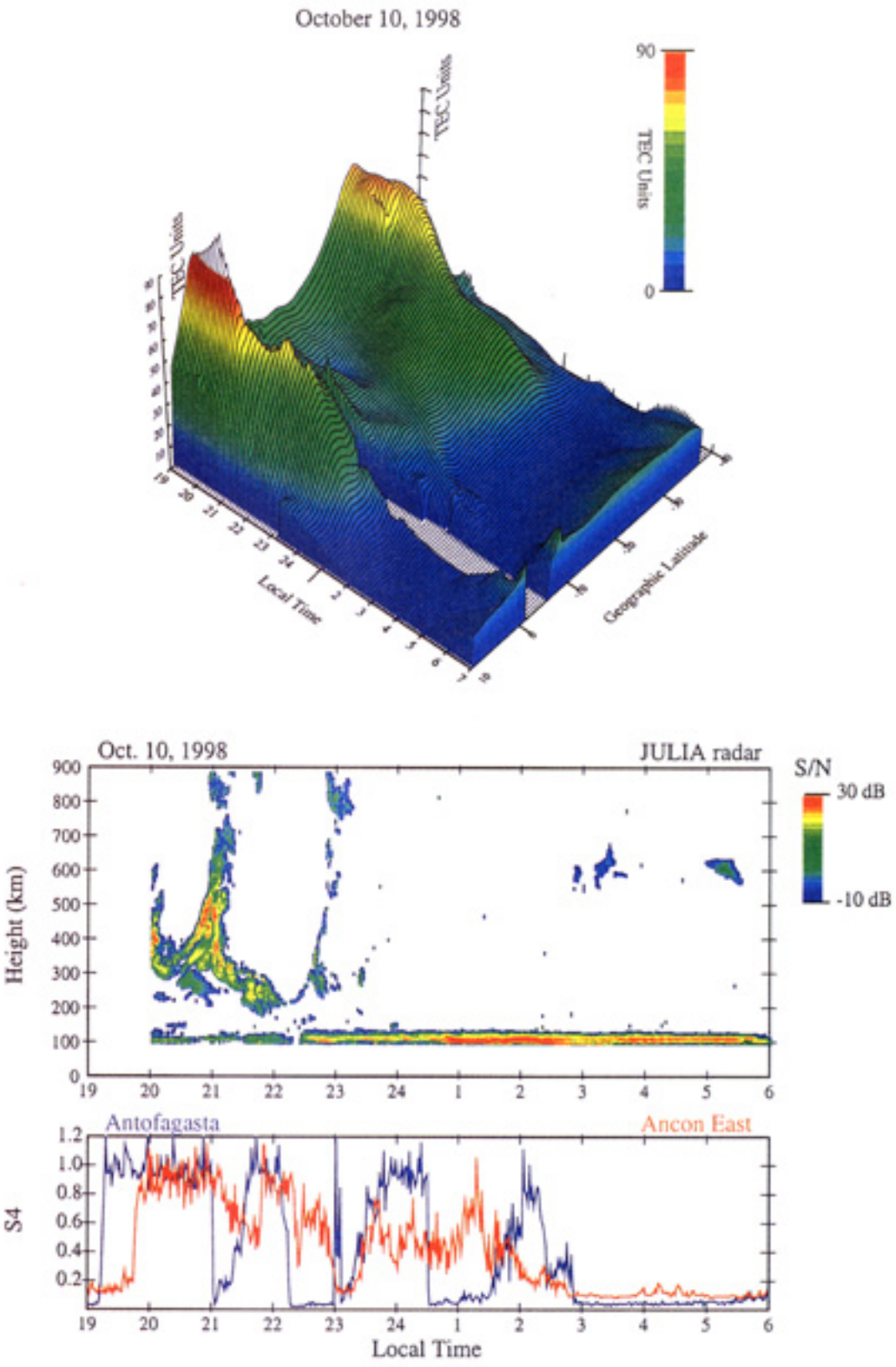

Plate 1. Data collected by the chain of GPS receivers, the JULIA radar, and two scintillation receivers on October 10, 1998. The top plot shows a three-dimensional view of the TEC values displayed as a function of geographic latitude and local time. The middle panel displays a color-coded plot of the magnitude of the coherent echoes gathered by the JULIA radar. The bottom panel shows S4 indices measured by the Ancon east and the Antofagasta west receivers. Note the presence of strong scintillations, plasma plumes extending up to 900-km altitude, and very pronounced anomaly crests.

is now known that several ionospheric conditions can help the RTI to develop. These are (1) the lifting of the *F* layer [*Farley et al.*, 1970; *Jayachandran et al.*, 1993; *Sastri et al.*, 1997], (2) a small or null transequatorial meridional wind [*Maruyama and Matuura*, 1984; *Maruyama*, 1996], (3) a simultaneous decay of the *E* region conductivity at both ends of the field lines [*Tsunoda*, 1985], (4) a sharp gradient at the bottomside of the *F* layer, and (5) penetration of magnetospheric fields. Furthermore, satellite in situ measurements have shown that some bubbles are able to attain supersonic velocities in the early stages of their development [*Agsson et al*, 1992; *Hanson et al.*, 1997]. In general, bubbles grow much faster than the time predicted by the RTI theory. These latter two facts suggest that the bubble initiation may involve the presence of a seed to make its development occur in a more explosive manner. *Kelley et al.* [1981], and *Hysell et al.* [1990] have indicated that gravity waves may be the seed that is required to initiate the growth of the plasma bubbles.

The development of ESF is closely linked to other processes that occur at local times near sunset, the time when most of the plasma bubbles are triggered. An important feature of the vertical drift is the sudden enhancement that occurs around 1900 LT and before the vertical drift turns downward. This feature was called the pre reversal enhancement (PRE) by *Woodman* [1970]. The occurrence of the PRE is important because this additional upward velocity displaces the *F* layer further upward, favoring the initiation of ESF. The full development of the PRE has been associated with the sunset decay of the highly conductive *E* layer [*Farley et al.*, 1986] and the time of reversal of the zonal thermospheric wind from a westward to an eastward orientation [*Crain et al.*, 1993]. *Basu et al.* [1996] presented the day-to-day variability of the PRE, observed during a prolonged campaign in South America, and suggested that the appearance of a well–developed PRE was associated with the onset of ESF. More recently, *Fejer et al.* [1999] have indicated that the vertical plasma drift may constitute the only observable that is required to predict the onset of ESF. A fully developed PRE can favor the growth of the RTI in three different ways: (1) It lifts the *F* region to more unstable altitudes, where the damping collisional term is smaller; (2) it implies the presence of an eastward electric field, which is also a destabilizing term in the generalized RTI; and (3) it speeds up the recombination at the lower altitudes of the *F* layer [*Hanson et al.*, 1983, 1986]. Therefore the presence of PRE is an important indicator of a posteriori development of ESF, but other characteristics of the equatorial plasma electrodynamics may also be equally important (e.g., transequatorial wind).

Another important feature of the low-latitude *F* region is an enhancement of the *F* region density that is observed at both sides of the magnetic equator. These have been called the Appleton (also named equatorial) ionization anomalies. They are the result of the upward motion of the plasma at the magnetic equator and its consequent diffusion obliquely along the magnetic field lines [*Hanson and Moffett*, 1966]. The total electron content (TEC) anomaly starts to develop as early as 1100 LT. It moves away from the equator with increasing local time, as the *F* region at the equator moves to higher altitudes, and it reaches a maximum development around 2000 LT. After 2100 LT the crests of the anomaly sometimes move rapidly toward the equator as the equatorial ionosphere moves downward. This latter process has been called "the reverse fountain effect" [*Sridharan et al.*, 1993; *Balan and Bailey*, 1995]. Several researchers have studied the morphology of the equatorial anomaly. *Walker et al.* [1994] used median hourly TEC latitude profiles obtained in Southeast Asia to account for the seasonal and solar cycle variability of the anomaly. These authors indicated that any asymmetry in the amplitude of the crests was due to the transequatorial wind blowing outward from the summer hemisphere and to the proximity of the subsolar point to the location of the largest crest. The asymmetry was more prominent during solstices but was sometimes observable at the equinoxes. On some evenings a strong resurgence of the anomaly takes place; this is probably related to a full development of the PRE. Consequently, precise measurements of the amplitude of both crests have decisive bearing on two of the processes that are intrinsically associated with the initiation of ESF: the vertical drift velocity and the transequatorial thermospheric wind. In addition, it has been suggested that the amplitude of the equatorial anomaly can be used as a precursor of the occurrence of ESF irregularities [*Raghavarao et al.*, 1988; *Sridharan et al.*, 1994]. *Sultan and Rich* [2000] and *Huang et al.* [2001] used in situ values of the density measured by the Defense Meteorological Satellite Program (DMSP) satellite to formulate a relation between the occurrence pattern of spread *F* and the amplitude and location of the crests.

In this paper we report measurements of the total electron content (TEC) performed with six GPS receivers. Five of them are strategically located south of the magnetic equator on the west side of South America. The geographic location of the six GPS receivers are Bogota (4.64°N, 74.08°W), Ancon (11.78°S, 77.15°W), Arequipa (16.47°S, 71.49°W), Iquique (20.27°S, 70.13°W), Copiapo (27.38°S, 70.34°W), and Santiago (33.15°S, 70.67°W). In this paper we first correlate important features of the latitudinal distribution of TEC to power maps collected by the JULIA radar (11.96°S, 70.4°W, and magnetic latitude (MLAT): 0.5°N). In section 3 we present a statistical analysis of the TEC latitudinal distributions and the S4 indices measured by two UHF spaced-receiver scintillation systems (SRSS). One of the SSRS is located at Ancon (subionospheric point at 10.66°S, 70.4°W, and MLAT: 2.17°N), and the other is placed at Antofagasta (subionospheric point at 25.4° S, 69.95° W, and MLAT: 11.3° S).

In the last few years, GPS receivers have been used to study several processes in the low– and high–latitude ionospheres. *Pi et al.* [1997] used a worldwide network of GPS receivers to monitor the instantaneous global distribution of large–scale ionospheric irregularities. *Coker et al.* [1995] used measurements of the rate-of-TEC index (ROTI) to resolve the spatial boundary of the auroral zone. *Kelley et al.* [1996] studied the performance of GPS systems during the passage of spread *F* depletions across the receiver's line of sight. In other instances, scintillations measured by GPS receivers have backed up and complemented other types of measurements [*Weber et al.*, 1996]. More recently, *Lunt et al.* [1999a,b] have used TEC values calculated from the GPS and Near–Infrared Mapping Spectrometer (NIMS) constellation of satellites to deduce the contribution of the plasmasphere to the total electron content. In all these cases the low cost of the GPS receivers, their portability, and easy deployment have

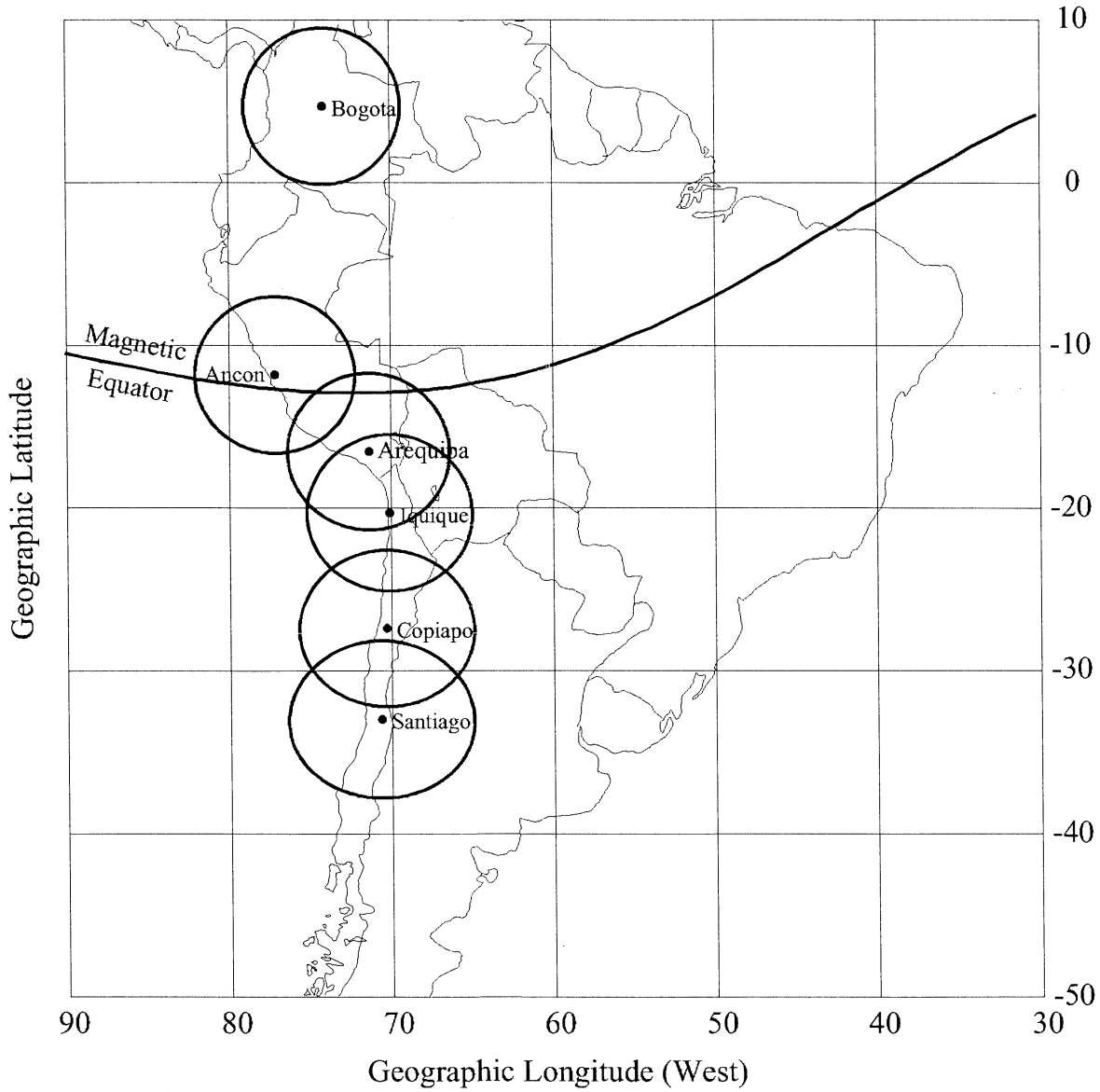

Figure 1. Site locations and field of view (30° elevation) of the six GPS receivers that were used in this study. Note the location of the magnetic equator and the existence of a region between -7° and 0° geographic latitude where TEC is not measured. The GPS receivers located at Arequipa, Iquique, Copiapo, and Santiago evaluate the TEC at latitudes south of the magnetic equator. The receivers situated at Bogota and Ancon diagnose northward of the magnetic equator.

prompted researchers to increase their usage during dedicated campaigns.

The scope of the paper is not to look for precursors of ESF plumes or scintillation activity but to examine the characteristics of the TEC latitudinal distributions when plumes are seen with the JULIA radar [*Hysell and Burcham*, 1998] and when UHF scintillations are observed simultaneously at Ancon and Antofagasta.

2. Data Sets

Figure 1 shows the location of all six GPS receivers. Four of the sites (Arequipa, Iquique, Copiapo, and Santiago) are situated south of the magnetic equator. Another one (Ancon) is placed close to the magnetic equator. The sixth receiver (Bogota) is located well north under the northern crest. Three different data sets were used in this study. The first data set consisted of the radar maps measured by the JULIA radar in 1998 (34 nights), the second set included S4 indices from the Ancon and Antofagasta scintillation systems for the same year, and the third set included TEC latitudinal distributions derived from the six GPS receivers, also for year 1998.

Plate 1 shows a particular sample from these three data sets corresponding to October 10, 1998, a day in which elongated plumes and strong scintillations were clearly evident. The bottom panel displays strong scintillations measured by the Ancon east (red line) and the Antofagasta (blue trace) receivers. The ray paths from these two sites intersect the *F* region ionosphere at virtually the same magnetic meridian plane but at latitudes separated by almost 12°. This particular geometry permits us to study irregularities that map to different apex altitudes. However, there are two differences. Ancon's observations are carried out using a 25° elevation angle compared to 65° for the Antofagasta measurements.

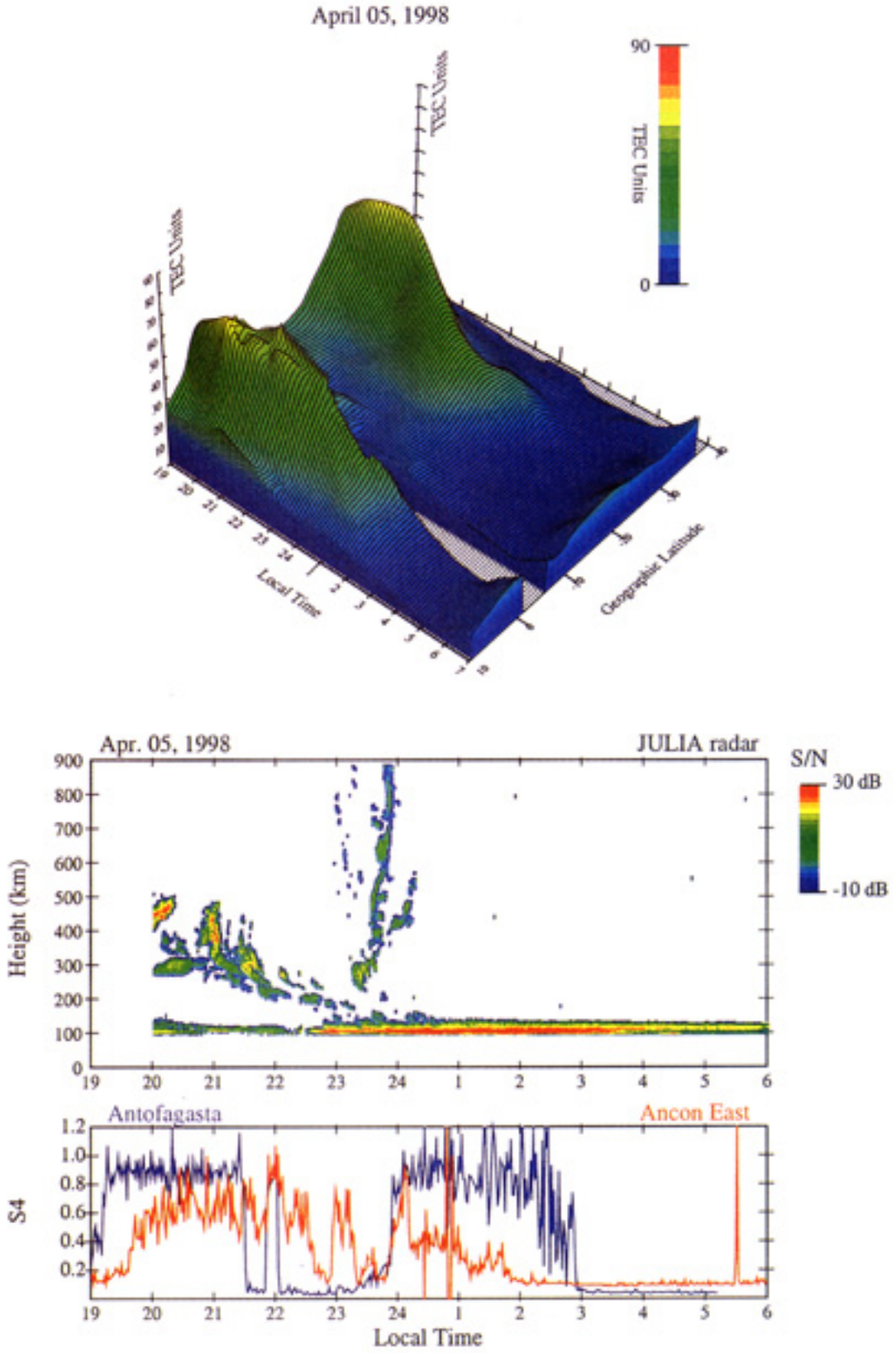

Plate 2. Same as Plate 1, but corresponding to April 05, 1998.

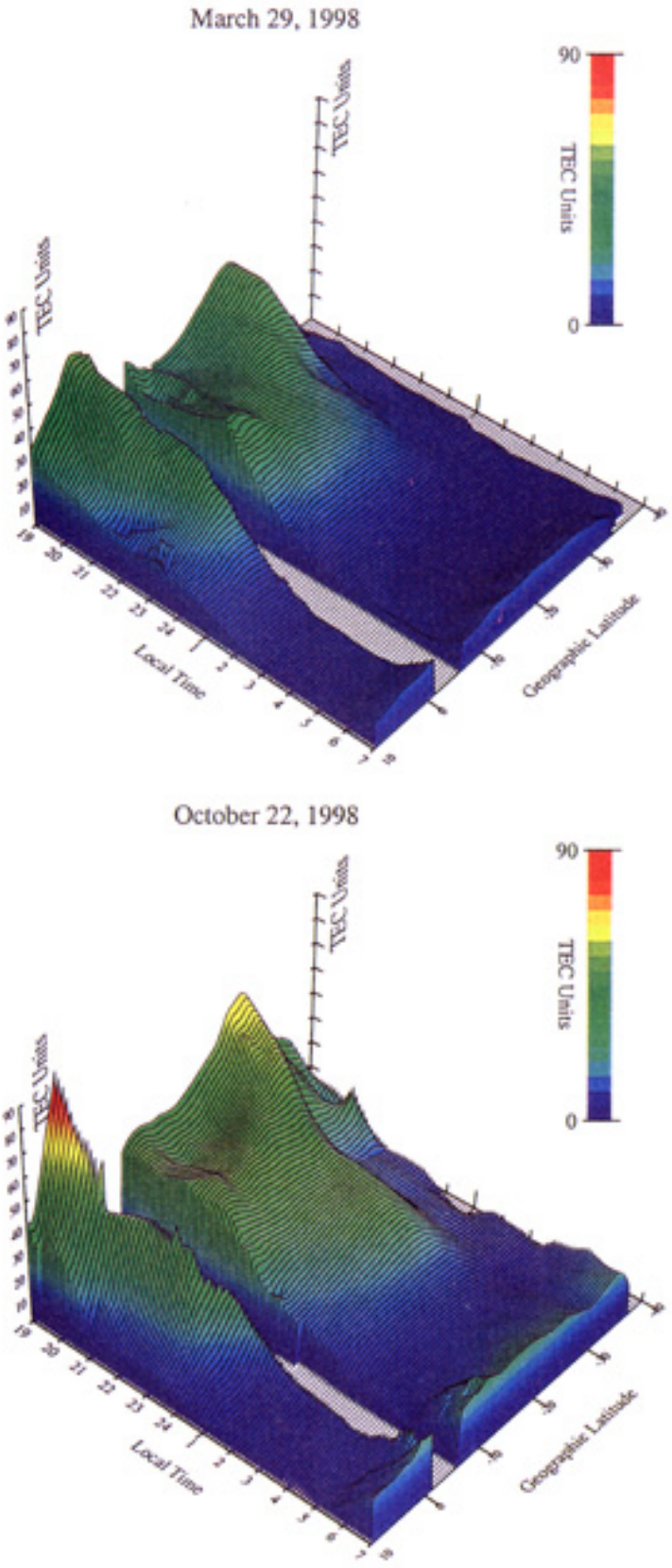

Plate 3. TEC values collected by the chain of GPS receivers on two nights when no scintillation and no coherent echoes were detected. Less pronounced and rapidly decaying crests are seen on these two days.

This makes the scintillations seen at Ancon originate over a longer ray path compared to the scintillations seen at Antofagasta. In addition, it is also possible that the ray path from the Ancon antennas intercepts more than one plasma bubble. It is also known that Antofagasta, being further closer to the southern anomaly crest, has a local plasma density larger than that of Ancon. All these reasons may account for the difference seen sometimes between the scintillation traces at each station. The middle panel of Plate 1 displays a series of plumes measured at Jicamarca using the JULIA radar on October 10, 1998. The first plume, seen at 2000 LT, reaches 600 km, and the other two (2100 and 2300 LT) extend up to at least 900-km altitude. All three plumes are seen connected to a bottomside layer. This layer shows a quasi-sinusoidal modulation in altitude; it is initially at 320 km, then it ascends to ~370 km, later lowers to 200 km at 2200 LT, and finally increases up to 280-km altitude at 2250 LT. The top panel is a three-dimensional view of the variability of the TEC as a function of geographic latitude and local time. The TEC curves were obtained by doing a two-dimensional (latitude and local time) regression analysis of the TEC values measured by all six GPS receivers. Prominent features in this panel are the two peaks at both sides of the magnetic equator (~-12° geographic latitude), indicative of a pronounced development of the Appleton anomaly. At 1900 LT both crests are larger than 75 TEC units, and the valley or trough is near 40 TEC units. Between 1900 and 2000 LT the amplitude of the peaks increases, and the trough decreases. At 2000 LT the northern crest exceeds 100, the southern anomaly peak reaches 80, and the trough decreases to 28 TEC units. At this local time the latitudinal TEC distribution presents the characteristics of the postsunset resurgence of the anomaly previously discussed by *Walker et al.* [1994]. These authors discussed a postsunset revival of the anomaly in terms of the occurrence of an intense PRE. The asymmetry in the amplitude of the anomaly peaks and the rapid decay of the northern peak may indicate the effect of a pronounced transequatorial meridional wind. Notice the absence of TEC measurements between 2° S and 6° S due to the lack of coverage by our limited network of GPS receivers.

Plate 2 has a layout similar to that of Plate 1. It displays the TEC distributions, the power map from the JULIA radar, and the time series of the scintillations measured on April 5, 1998. The bottom panel shows that the scintillations at Ancon were much weaker than the scintillations at Antofagasta. S4 values at Antofagasta reached saturated values, and at Ancon the scintillations varied between 0.8 and 0.4. In addition, the onset of scintillations at Antofagasta preceded that at Ancon by 40 min. As mentioned above, these discrepancies may be attributed partially to differences of the geometries being intersected and the variability of the local density at the subionospheric intersections. The JULIA data present a series of small plumes extending up to 500 km between 2000 and 2200 LT; these miniplumes are followed at 2350 LT by a tall and narrow plume extending from 230-km altitude up to >900-km altitude. There is also a bottomside layer connecting the lower boundary of the plumes, which is observed to be continuously lowering in altitude and seems to end at the equatorial electrojet. The TEC plot shows a pattern of two well-defined peaks, which are increasing in amplitude until 2200 LT. After this time they start decreasing and finally fade at 0100 LT. Both peaks have almost similar amplitudes with maximum values close to 65 TEC units. Similar to Plate 1, the peak/trough ratio at the time that the plasma plumes are observed is larger than 3.

Plate 3 illustrates two cases when neither scintillations nor radar echoes were detected. During these two days both anomaly peaks are evident; nevertheless, they do not posses a large amplitude like the cases shown in Plates 1 and 2. Important features of the TEC latitudinal distributions are the relatively larger values at the trough and the absence of an early evening reinitiation of the fountain effect as seen in Plates 1 and 2. The TEC distribution for March 29, 1998 (top panel), is approximately symmetric with respect to the magnetic equator. On this day both anomaly peaks decay before local midnight. The trough increases from 28 TEC units at 2000 LT up to 35 units at 2200 LT. This postsunset increase of the trough density is indicative of a reverse fountain effect in which plasma density from the anomaly peaks is transported back to the magnetic equator through a diffusion process in which plasma flows along and up the field lines. The bottom panel of Plate 3 shows the anomaly corresponding to October 22, 1998, a day when both peaks developed asymmetrically. The TEC value at the trough varies between 37 units at 2000 LT and 40 units at 2200 LT. Both anomaly crests decay very rapidly after sunset, and at 2100 LT they are almost nonexistent. At sunset time (1900 LT) both TEC distributions of Plate 3 present a crest/trough ratio less than 2.

3. Data Analysis

We have binned the TEC latitudinal profiles for two opposite states of the equatorial ionosphere. The first state consists of an ionosphere populated by deep and altitude-extended plasma depletions, and the other state is associated with a uniform and undisturbed ionosphere. To determine the altitude extension of the plasma depletions (ESF) we used data from two experimental techniques. First we have employed power maps of coherent echoes collected by the JULIA radar to indicate the maximum altitude of the plasma plumes for all the nights the radar operated in 1998. When the radar echoes surpass 550-km altitude, as the examples shown in Plates 1 and 2, they were counted as nights of deep bubbles. Secondly we have used concurrent observations of strong scintillations by the Ancon east and Antofagasta receivers as a proxy for the occurrence of plumes extending, at least, up to 550-km altitude. It has been demonstrated that an *F* region located at, say, 350-km altitude at Antofagasta maps above 550-km altitude at the magnetic equator [*Basu et al.*, 1996]. By considering two completely opposite states of the equatorial ionosphere, a very turbulent one (altitude-extended plumes) and a second state of an undisturbed ionosphere, we expect to find significant differences in the characteristics of the TEC latitudinal distributions. A third state consisting of bottomside layers and/or miniplumes (< 500-km altitude) is not considered in this study.

3.1. Statistics of TEC Distributions Binned According to JULIA Observations

The top panels of Figure 2 show TEC latitudinal distributions measured at 2000 LT for all the nights in 1998 that the JULIA radar observed plumes reaching at least 550 km-altitude. The bottom panels show the TEC distributions for nights when JULIA recorded bottomtype layers or a total

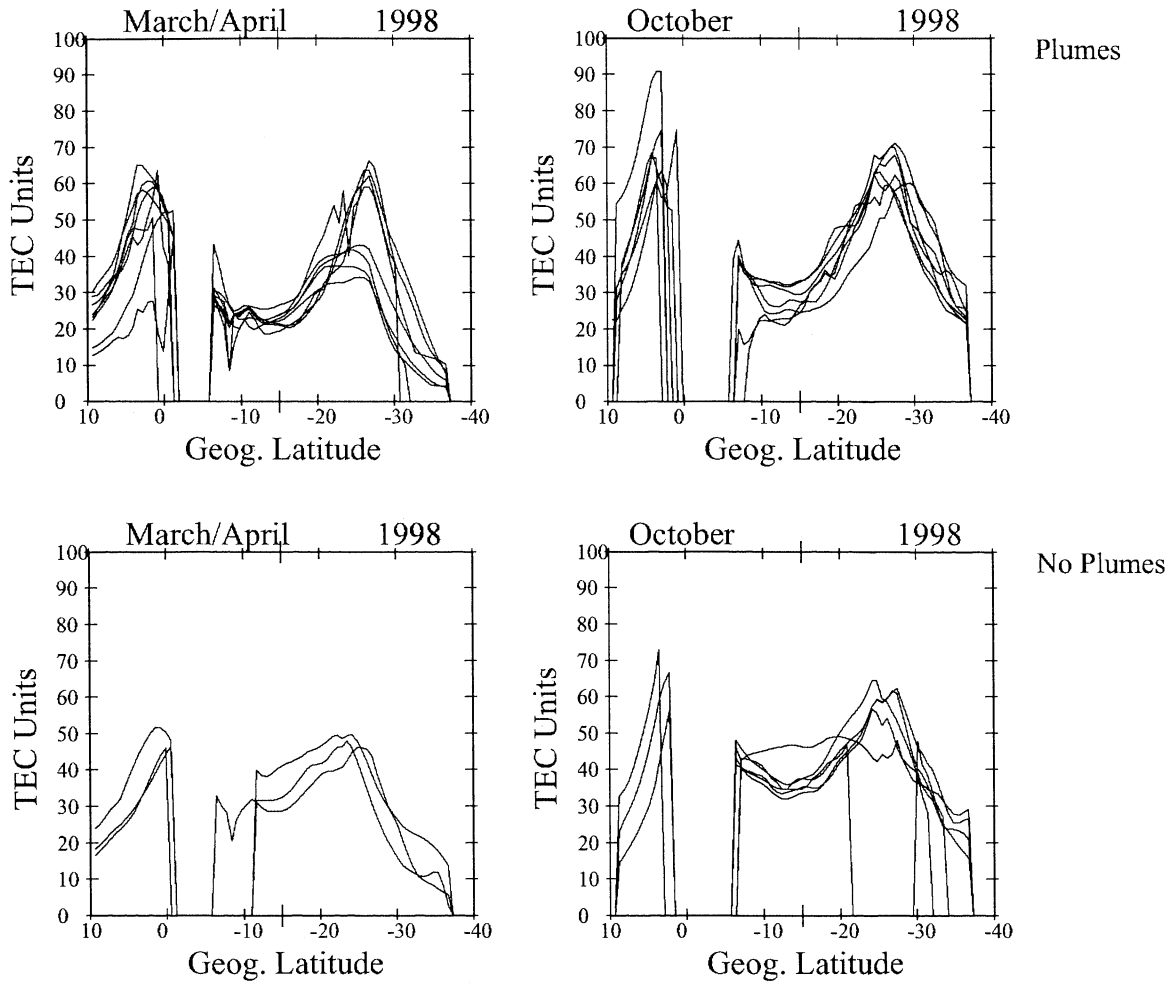

Figure 2. Latitudinal TEC distributions for the equinoxes binned according to the occurrence or not of plumes. Note the difference between the TEC distributions shown in the top panels, corresponding to days of plasma plumes, and the bottom panels for no-plume days. The TEC curves in the top panels show pronounced and narrow crests. The bottom panels exhibit smaller and wider crests.

absence of spread *F* echoes. All four panels (plumes and no plumes) clearly show the double-humped distribution of the low-latitude density and TEC, that are quite typical in the afternoon and early evening [*Doherty et al.*, 1997]. Another distinguishable feature of the TEC distributions is the existence of a trough, which almost always resides at latitudes close to the magnetic equator. Both crests are located at magnetic latitudes varying between 12° and 18° but are not always placed symmetrically with respect to the magnetic equator. Careful comparison of all four panels reveals that the TEC distributions present some significant differences depending upon the presence/absence of elongated plumes. The TEC value at the trough varies between 20 and 30 TEC units during plume days compared with 40 units for no-plume cases. The crests are usually higher and narrower and show steep latitudinal gradients during plume days; they are smaller and shallower during no-plume days. Therefore the ratio of peak/trough is larger during plume cases than it is during events that contain no plumes. Finally, we also noticed that the crests of the TEC anomaly are displaced to higher magnetic latitudes during plume events. The amplitude of the anomaly crests during the month of October peaks 10-15 TEC units higher than that during March/April. This may be partially because of the higher solar flux intensity in October 1998 or an intrinsic difference between both equinoxes. The intensity of the solar flux was 116 (in units of 10^{-22} W m^{-2} Hz^{-1}) during October and 108 units during April.

3.2. Statistics of TEC Distributions Binned According to Scintillation Observations

Figure 3 shows the latitudinal distribution of TEC taken at 2000 LT for all plumes and no-plume nights when at least four GPS receivers were operating. It is evident that the season exerts a strong control on the formation of the anomalies and on the maximum amplitude of the latitudinal distributions. During the equinoctial months (March, April, September, and October), typical distributions showing well-defined crest-trough-crest features are seen almost everyday. During these months the TEC amplitudes are also the largest, reaching values in excess of 80 TEC units. During the months of February, May, August, and November (transition months) the TEC distributions show, on some days, the presence of the anomalies, but on many other days the TEC profiles are flat, or only a weak anomaly seems to have developed. During these months the peak TEC values are also smaller than the maximum equinoctial values. Excluding December, the solsticial months (January, June, July, and

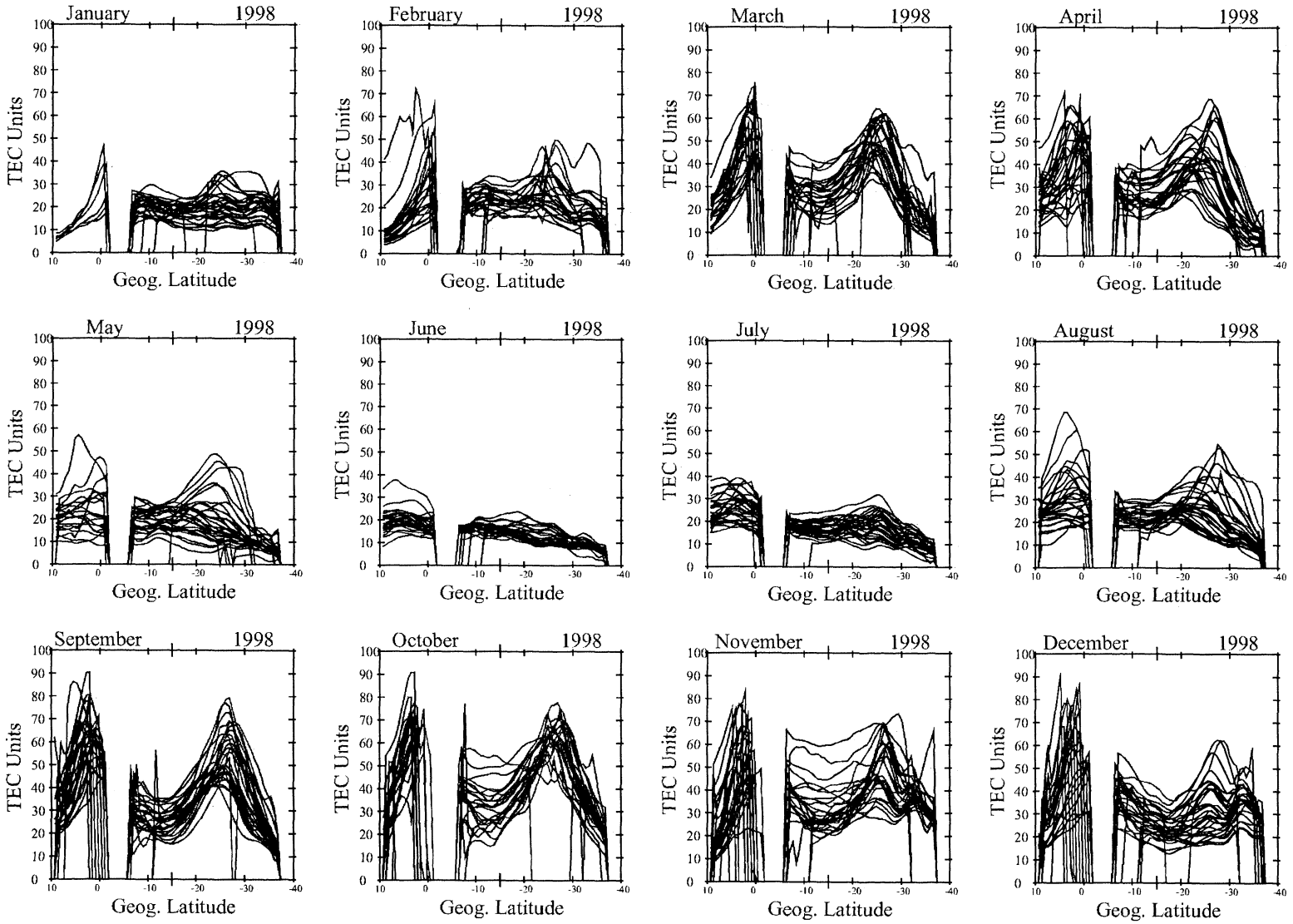

Figure 3. Latitudinal TEC distributions measured at 2000 LT for all days when at least four GPS receivers were operating. Each panel corresponds to one month of observations during 1998. Note the seasonal variability in the occurrence and amplitude of the crests.

December) show TEC distributions without an anomaly crest. During these months the TEC distributions are less than 30 units at all latitudes. They show a peculiar trend of TEC values decreasing from the north toward the south. In general, there exists a day-to-day variability of the TEC distributions, with the smallest values occurring during the solsticial months. As explained in section 5, we believe that this difference in the TEC distribution, observed at 2000 LT, is a consequence of the monthly variability of the equatorial vertical drifts, the meridional neutral wind, and the subsolar location. The seasonal variability of the presence/absence of the anomaly agrees well with the seasonal occurrence of the evening prereversal enhancement seen at Jicamarca during solar minimum conditions [*Fejer et al.*, 1991].

Figure 4 displays the TEC latitudinal distributions only for days when scintillations were seen at both scintillation stations (Ancon and Antofagasta). The anomaly peaks are fully developed every day that scintillations were observed in March, April, September, October, and during most of the cases in November (equinoctial events). Most of the TEC distributions during the months of January, February, and December do not show the presence of the anomaly crests. On a few days only a very weak anomaly or an asymmetric trace is observed (we have called these events the December solstice cases). However, it is conceivable that a weak density anomaly, a sharp gradient in the bottomside density, or a high altitude of the *F* region has occurred although no TEC peaks are evident in our data. The absence of a TEC crest suggests that during these months the fountain effect and the implied lifting of the *F* layer may not play a prominent role in the onset and in the corresponding development of plasma "plumes" during this season. During the months of May, June, July, and August (June solstice), scintillations (and ESF) are seen only rarely in the American sector [*Basu and Basu*, 1985]. During the month of August, ESF events are accompanied with TEC distributions, presenting characteristics almost similar to the equinoctial cases. During the months of June and July there is only one case per month of ESF, which contains weak anomalies.

Figure 5 shows the TEC latitudinal distributions when no ESF was seen at both stations. Not surprisingly, the anomaly crests are still present for most of the months. In fact, they are observed in all the seasons, in which we observed anomaly peaks in Figure 4 (scintillation cases). However, close inspection of the TEC latitudinal distributions shows prominent differences between the plume and no-plume cases, similar to Figure 2. The no-ESF events seen during the equinoxes show a much higher value in the valley and weaker anomaly peaks than the ESF events (Figure 4). The December solstice cases show again a flat distribution or, in very few cases, a modest anomaly. The numerous events of no ESF that occurred during the June solstice show mainly a flat distribution or very weak anomalies as seen during the months of May and August. In section 4 we parameterize the TEC distribution in order to estimate quantitatively the differences that are related to the ESF activity.

3.3. Statistics of the Time Differences of TEC Distributions

To explore the possibility that the TEC distributions for 1800 LT and earlier times may present different characteristics as a function of the presence/absence of scintillations, we inspected all the TEC distributions between 1500 and 1800 LT. We found no evident distinguishable features; in fact, even during the equinoxes there was no clear difference depending upon scintillation activity. This seems to imply that the ESF onset was probably mostly related to the evolution of the low-latitude density between 1800 and 2000 LT. On the basis of this hypothesis, we carefully looked at the variability of the TEC distributions in this 2-hour period. We subtracted the TEC distribution measured at 1800 LT and the values at 2000 LT, or expressed in mathematical form,

$$d\text{TEC} = \text{TEC}(1800) - \text{TEC}(2000),$$

In this format, positive values indicate a temporal reduction or attenuation of the TEC distributions; negative *d*TEC values indicate a growth or enhancement in TEC. There are some striking distinctions between Figures 6 and 7. Figure 6 shows *d*TEC values for all nights in 1998 when scintillations are seen at both Ancon and Antofagasta. The prominent feature is the strong latitudinal variability in all these curves. During the months of March, April, and from August to December there exists a large *d*TEC value (>20 TEC units) at latitudes near the magnetic equator (-12° geographic latitude) and much smaller values (in many cases negative) at latitudes near the anomaly peaks. This variable pattern indicates that the value of the TEC crests increase and that the TEC trough diminishes during days when ESF occurs. For the solsticial months (January, February, June, and July) there is an indication of a TEC increase near the anomaly peaks, although it is not so pronounced as that observed during the equinoxes. Figure 7 displays *d*TEC values corresponding to days when no scintillations were present. Almost all the *d*TEC curves are quite uniform or present high positive values near the anomaly crests as seen in October and November. The amplitude at the magnetic equator rarely exceeds 20 *d*TEC units, and there are almost no negative *d*TEC values at the crests. These almost flat *d*TEC distributions imply that during 1800 and 2000 LT there exists an almost constant decrease of the TEC at the latitudes covered by the GPS receivers.

4. Parametric Characterization of the TEC Latitudinal Distributions

Figure 8 shows a schematic representation of the low-latitude TEC distribution along a magnetic meridian. In this idealized example the TEC trough is located at -12° geographic latitude. Both crests are displaced 14° away from the magnetic equator, and the peak of the northern crest is larger than the southern. We have observed that this TEC configuration is not uncommon; it occurs quite often during the Southern Hemisphere summer season (December solstice), when a transequatorial wind blows northward. Figure 8 also displays all the parameters that can be used to fully characterize the TEC latitudinal distributions. These quantities are the amplitude and locations of the trough and crests and the integrated excess value of the TEC within the anomaly crests (the southern crest integrated value is depicted here as a shaded area). One of the goals of the present study was to investigate the possibility of parameterizing the TEC latitudinal distributions and to examine if these parameters could be related to the presence/absence of ESF. The main difficulty that we encounter in the present array of GPS receivers is that only one receiver is placed at latitudes north of Ancon to cover an 18° latitudinal span. Thus we restricted

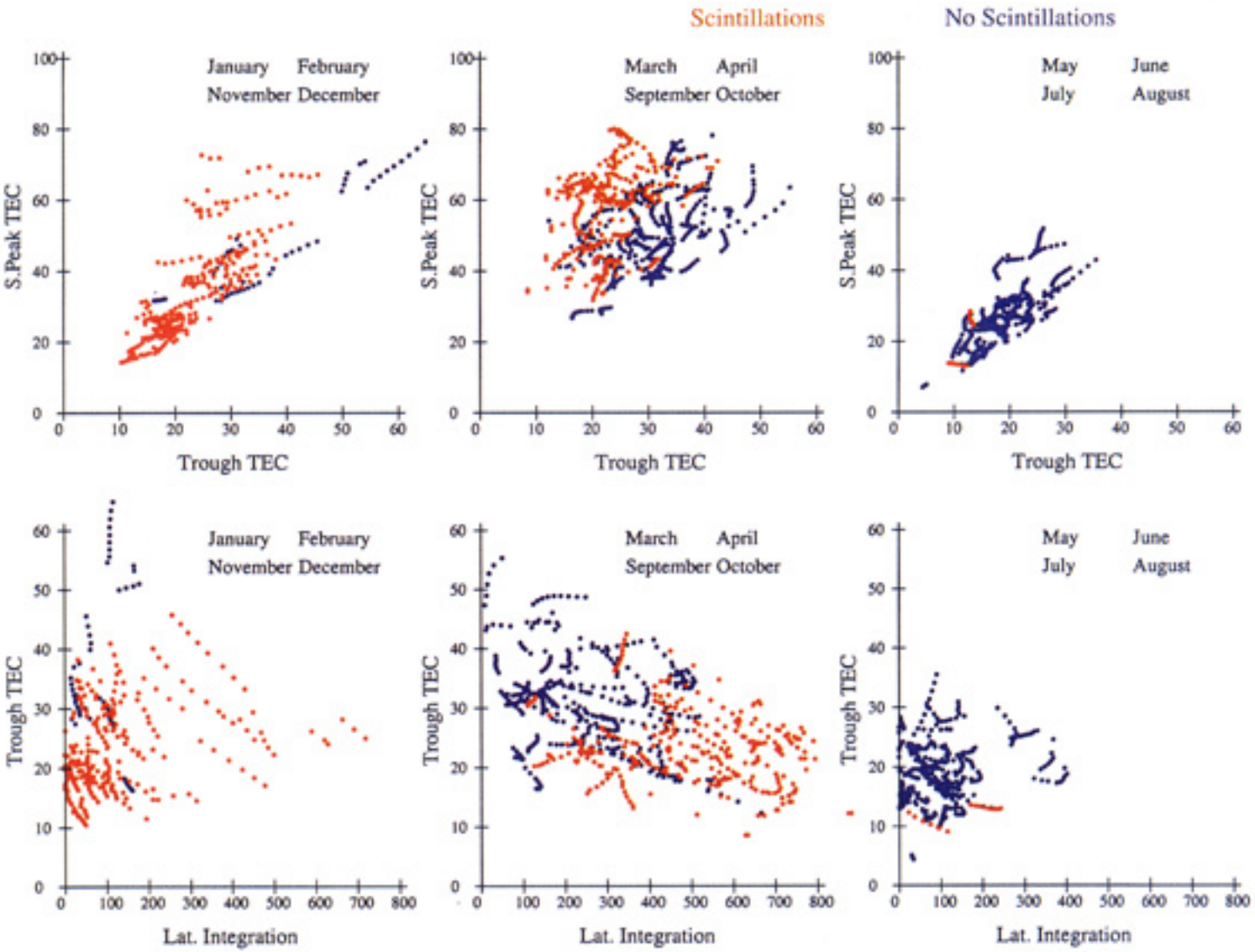

Plate 4. Mass plots of selected parameters extracted from the TEC latitudinal distributions. The dots have been color-coded to represent cases of scintillations (red dots) and no scintillation (blue dots). The top panels show the variability of the TEC peak value of the southern crest versus the value of the trough. The bottom panels display TEC trough values as a function of the integrated TEC value under the southern crest.

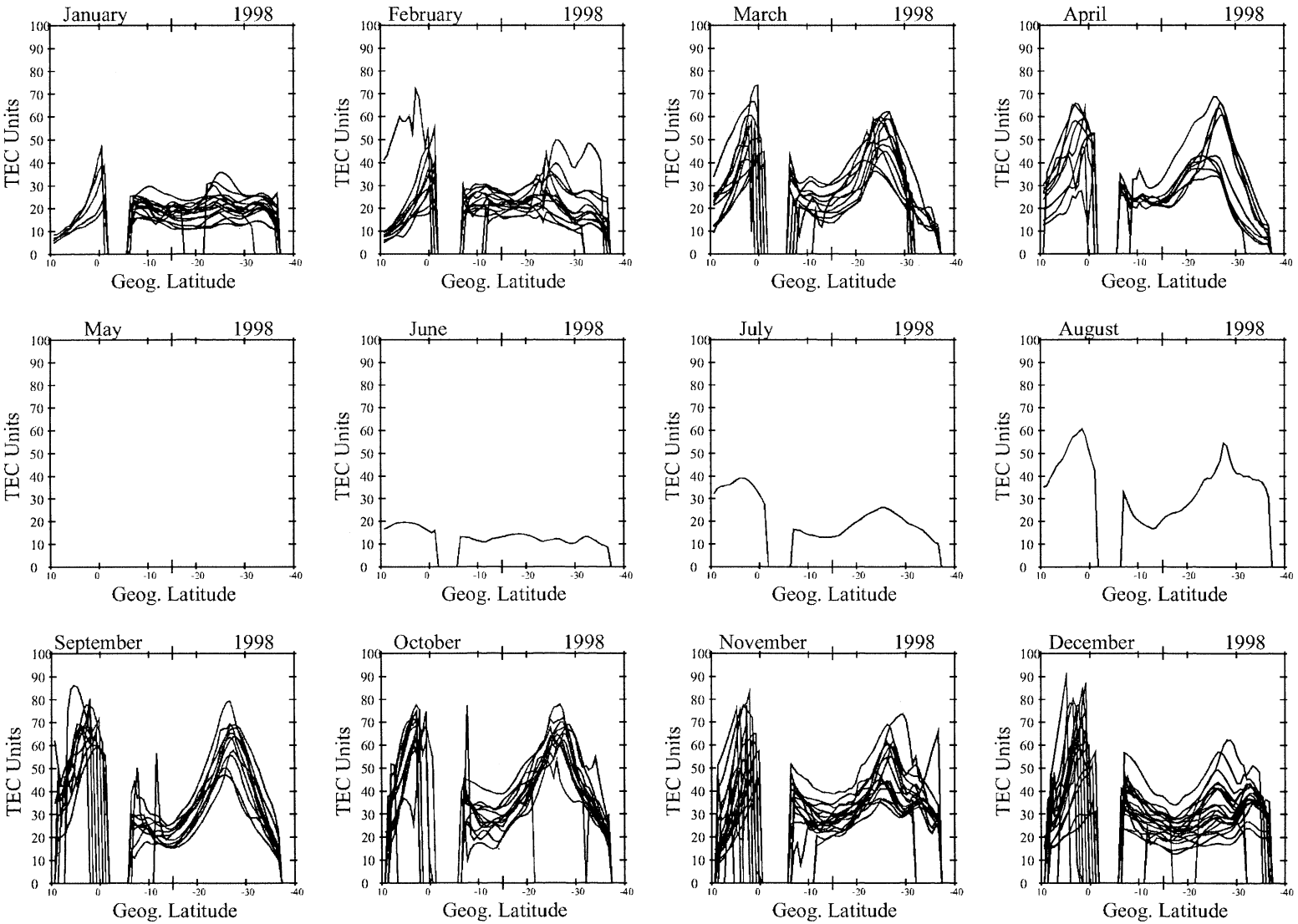

Figure 4. Same as Figure 3 but for nights when scintillations were observed at the Ancon and Antofagasta stations. During the equinoxes the distributions present pronounced crests and a low trough.

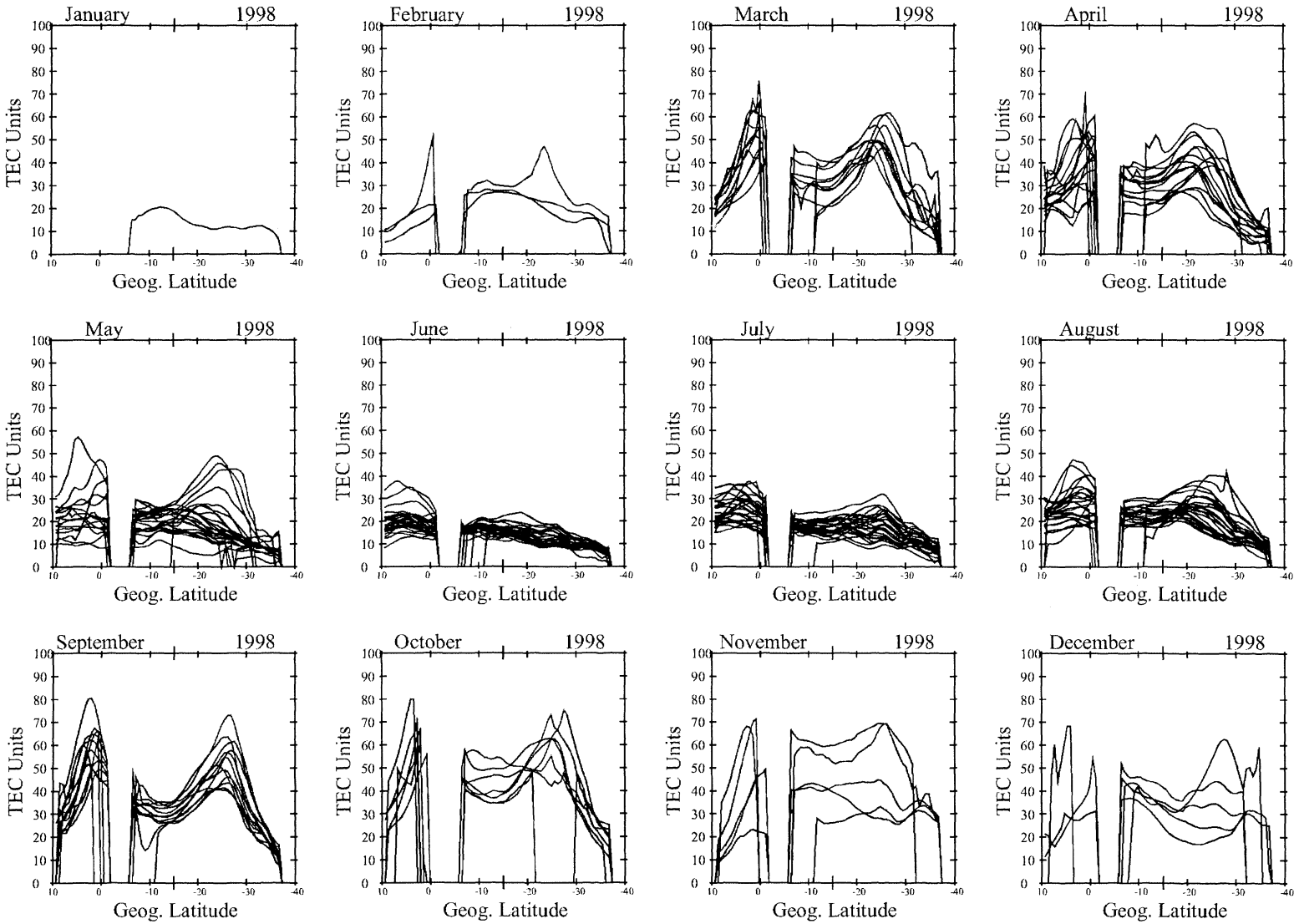

Figure 5. Same as Figure 3, but for nights when scintillations were observed neither at Ancon nor Antofagasta. The equinoctial TEC distributions usually show mild crests and a higher trough.

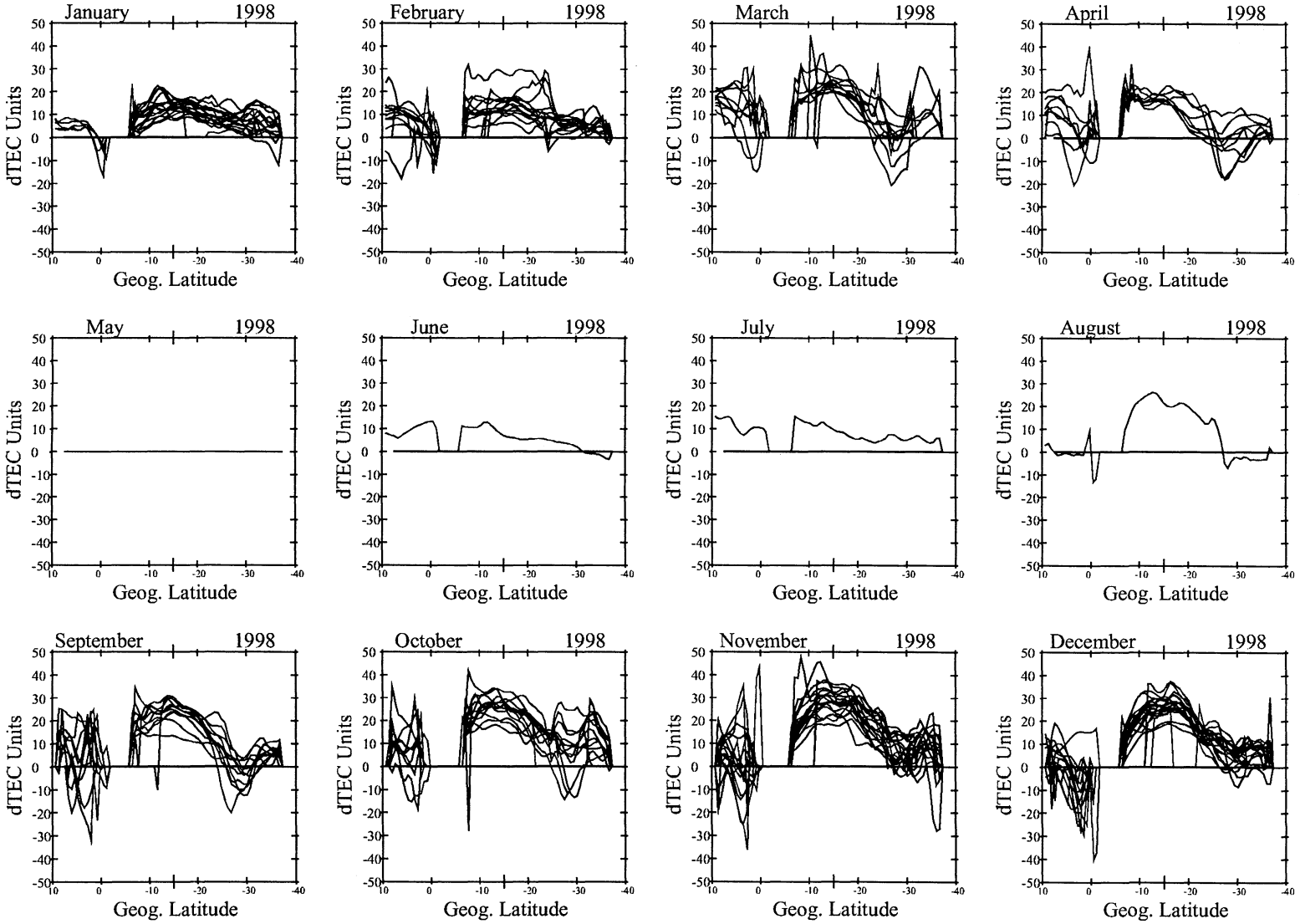

Figure 6. Time difference distributions obtained by subtracting the value of the TEC distributions corresponding to 1800 LT and the curves for 2000 LT. Only days in which scintillations occurred at both stations are plotted.

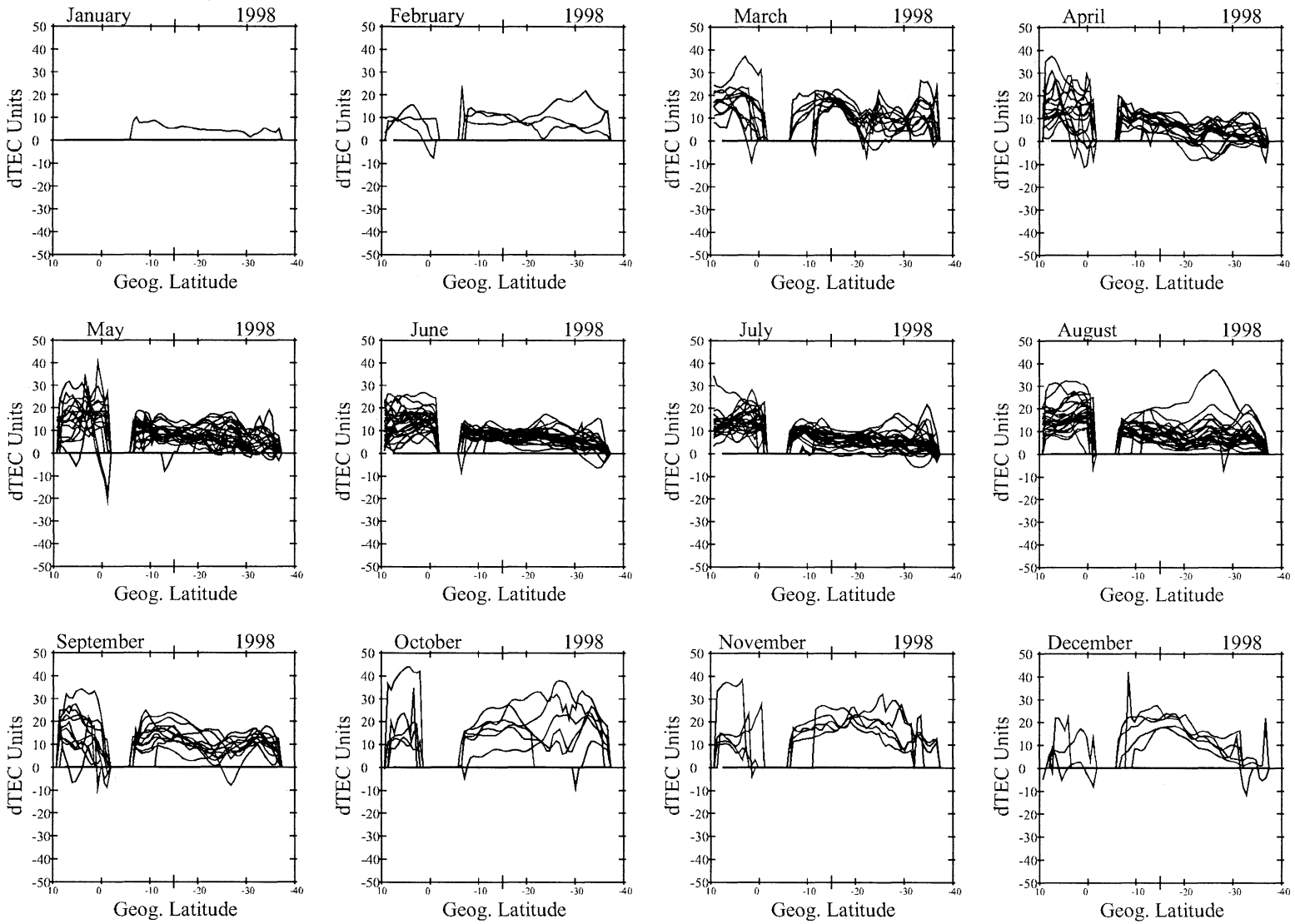

Figure 7. Same as Figure 6, but for days of no scintillations at both stations.

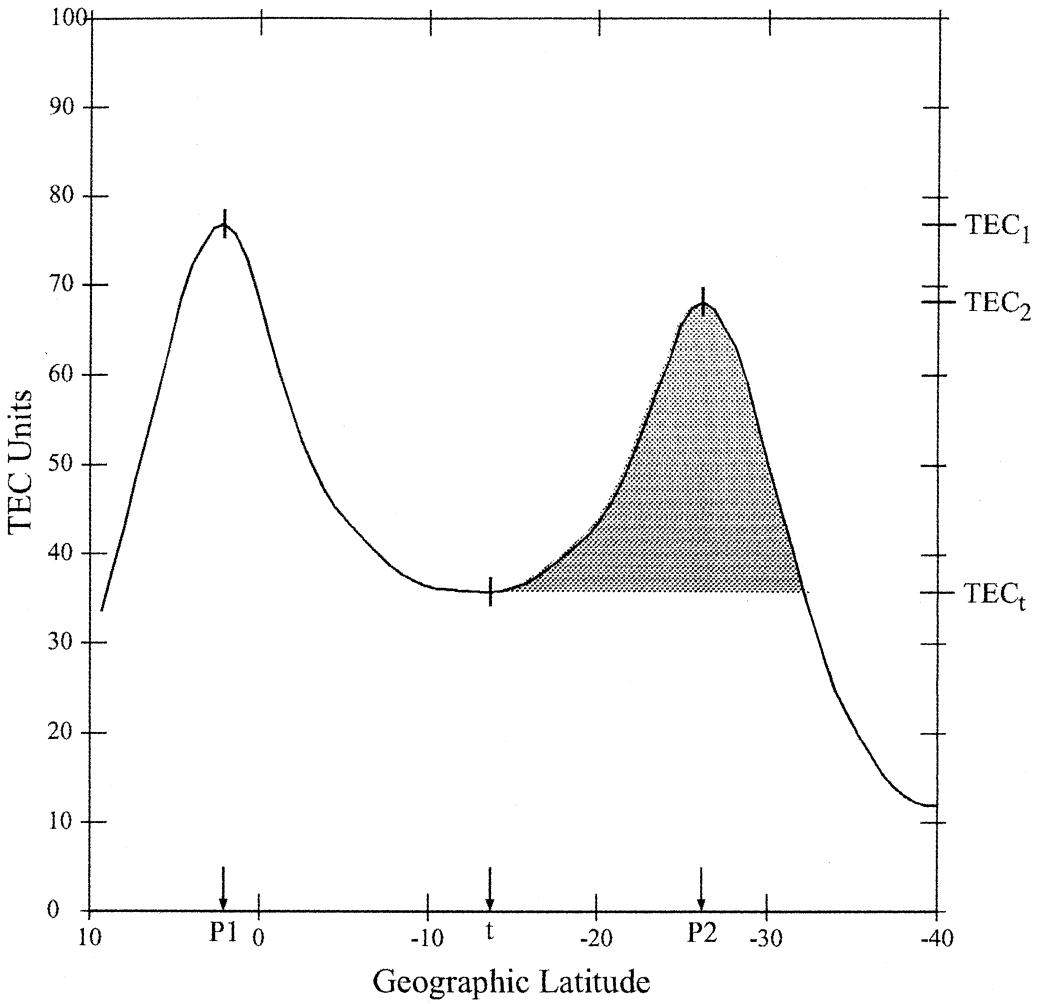

Figure 8. Sketch of a typical latitudinal distribution of TEC values. The arrows in the bottom part of the figure indicate the geographic locations of the crests (P1 and P2) and the trough (t). The shaded area in the southern crest serves to show our interpretation of the integral value of the crest. See text for details.

the TEC parameterization only for values measured at latitudes south of −5° geographic latitude. The amplitude of the trough, the peak value of the southern crest, and the latitudinal integration of the TEC near the southern anomaly were the only parameters selected to characterize the TEC distributions. The latitudinal integration of excess TEC is related to the total amount of ionization that diffuses along the field lines as the result of the equatorial fountain effect and the transequatorial plasma transport produced by the meridional wind.

The top panels of Plate 4 show mass plots of the amplitude of the southern crest versus the TEC value at the trough at 2000 LT. The bottom panels display the trough amplitude as a function of the TEC latitudinal integration, again at 2000 local time. The three panels in each row correspond to December solstice, equinoxes, and June solstice seasons, respectively. Data from four months are included in each panel; the months included are printed in the upper right corner of each frame. The red dots indicate cases when scintillations were observed at Ancon and Antofagasta. They should equally correspond to cases when plumes extended from the bottomside of the *F* layer up to 550-km altitude. The blue dots imply events when no scintillation is observed at either site or cases of no ESF. The well-known seasonal occurrence of scintillations is evident in these panels. More red dots are seen during the equinoxes and the December solstice, and the majority of blue dots occur during the June solsticial months. It is important to mention that during some seasons, like the December solstice when the occurrence of scintillations nears 50%, there are not many blue dots, because the TEC distributions are constant in latitude and the processing software fails to compute the location of the crests and the trough.

The frames corresponding to the equinoxes (middle panels) contain the best statistical significance in each of the rows. Close examination of these panels reveals the existence of a weak separation between the red and blue dots in the top row. However, there is a preference for the scintillation (red) dots to have smaller TEC values at the trough than the no-ESF (blue) dots, but there exists a significant overlap. Better separation is observed in the equinoctial data plotted in the bottom row. No-ESF dots are grouped for low values of the latitudinal integration and high trough TEC values. Opposite to this, the ESF dots correspond to high latitudinal integration values and low trough TEC numbers. In summary, the latitudinal integrated value and the amplitude of the trough

are good parameters that can be closely associated with the occurrence of ESF.

5. Discussion

The TEC values presented in this paper were calculated following a series of processing stages, which are potentially affected by errors. Here we briefly review the main characteristics of this analysis. The TEC calculation is based upon the well-known property of the ionospheric and plasmaspheric densities to produce a delay in the pseudorange and an advance in the phase of the GPS signals. These two basic quantities (pseudorange and phase), which are commonly provided by dual-frequency GPS receivers, are combined to obtain the absolute value of the TEC. However, the pseudorange is affected by multipaths, and the phase is affected by cycle slips. In addition, it is necessary to know the satellite transmit bias and the receiver system bias. The first stage of the GPS signal processing consists of finding the value of these biases and eliminating the negative effect of multipaths. This was accomplished using the self-calibration of pseudo-range errors (SCORE) program developed by *Bishop et al.* [1996, 1997]. This algorithm uses the same measurements of the ionospheric delay to derive the sum of the receiver and the satellite biases. The self-consistent calibration is achieved by considering conjunctions of two satellites crossing the same ionospheric volume, in a common latitude and local time sector, and assuming that the TEC value is equal in the common volume. This operation is repeated for all the satellite crossings that are observed in a 24-hour period. We use the SCORE program to conduct independent calculations of the biases for all six stations for each day of the year, when at least 4 hours of data had been collected. Day-to-day variations in the biases were no more than a few TEC units. Nevertheless, the receiver bias is subject to seasonal changes, which can account for several TEC units. To obtain this monthly trend, we fitted a quadratic function to the diurnal values of the biases for each satellite and for each station. The new fitted biases were then used to recalculate the values of the TEC. The line-of-sight (oblique) TEC values were also merged with ephemeris values of the sub-ionospheric locations to compute the equivalent vertical TEC. Finally, values from all six stations were put together using a two-dimensional regression analysis, eliminating cases when cycle slips had not been corrected or when unreasonably large values of the TEC were obtained. Another likely source of error is the latitudinal variability of the plasmasphere contribution to the TEC. We minimized this effect by restricting the data that are employed in the regression analysis to satellite elevations larger than 35°. The proof that the plasmasphere density does not alter our results is the fact that a very good agreement was obtained between the TEC values measured at different stations and during latitudinal conjunctions.

The TEC latitudinal profiles of Plates 1 and 2 (corresponding to ESF nights) have indicated that during the early evening the value of the TEC at the trough rapidly decreases; simultaneously, the amplitude of the crests increases or remains unchanged until 2200 LT. We believe that this behavior can be explained in terms of a postsunset revival of the fountain effect driven by the prereversal enhancement of the *F* region vertical drift velocity. Both plots of Plate 3 (corresponding to no-ESF nights) have shown that during these nights the anomaly crests were present, but their amplitude and temporal behavior were different as compared to the evolution seen in Plates 1 and 2. The amplitude of the crests of Plate 3 starts decreasing near or before 1900 LT, and the TEC value at the trough increases between 1900 and 2300 LT. This latter behavior has been explained by *Balan and Bailey* [1995] as the action of the reverse fountain effect driven in this case by a downward vertical drift and a plasma flow from the anomalies toward the trough. The lowering of the equatorial *F* region produces a pressure imbalance along the field lines, which makes the plasma located at the anomalies diffuse toward the equator by moving up the field lines.

Figure 6 indicates that during the equinoctial and December solsticial months when scintillations are simultaneously observed at both stations, the revival or resurgence of the fountain effect occurs. Figure 7 suggests that when scintillations do not occur at both stations, either a latitudinal uniform decay of TEC or a reverse fountain effect was the typical pattern. This evidence supports a previous study reported by *Fejer et al.* [1999], in which they indicated that the vertical drift velocity was the controlling parameter in the generation of spread *F* irregularities. These authors associated the occurrence of large prereversal enhancements of the vertical drift with the initiation of strong coherent echoes, and early downward drifts with the absence of unstable layers. We suggest that the same upward drift, which drives the *F* region to higher and more unstable altitudes, is also responsible for the postsunset revival of the fountain effect and that the occurrence of the early downward drift becomes the driver of the reverse fountain effect. Thus Figures 6 and 7 are indirect proof of the control that the equatorial electrodynamics, and specifically the vertical drift velocity, exert upon establishing the right conditions for the development of ESF. *Balan and Bailey* [1995] suggested that the reverse plasma fountain could also cause the formation of plasma bubbles and irregularities at high altitudes. We found no indication of this effect in the data for 1998 that we analyzed. However, it is possible that this effect is quite rare or solar cycle dependent.

During the June solstice we found that the TEC distributions for scintillation cases were similar to the distributions corresponding to days without scintillations. However, in this season, scintillations were observed on only two days. This fact clearly limits the statistical significance of any conclusion that could be drawn from the characteristics of the TEC distributions.

Several studies have indicated the importance of the altitude of the *F* region in the formation of the ESF irregularities. *Farley et al.* [1970] suggested the existence of an altitude threshold that was required for ESF irregularities to evolve. *Jayachandran et al.* [1993] concluded that the altitude of the *F* layer, as determined by the time history of the prereversal enhancement of the vertical drift, was the deciding factor for the onset of spread *F*. These authors proposed that the altitude threshold for ESF to occur varied from 450 km for a solar flux equal to 120 units to 350 km for a flux value of 70 units. In this study we have been able to compare the onset of scintillation with another integrated effect of the vertical drift, namely, the amplitude of the anomaly crest.

One of the highlights of this study has been our ability to calculate the geographic locations of the trough and the peak

of both anomaly crests. We found that the peaks were not always situated symmetrically with respect to the magnetic equator; neither was the trough always centered just at the equator. Similar distributions have been shown by *Walker et al.* [1994], based on measurements conducted in southeast Asia, and *Vladimer et al.* [1997] using measurements conducted with the TOPEX/Poseidon satellite. *Balan and Bailey* [1995] found a weak TEC anomaly in their simulations of the equatorial ionosphere and plasmasphere. These authors obtained crest/trough ratios less than 2, much less than the ratios equal to 5 found in this study. Thus our TEC distributions are consistent with previous experimental measurements but not with previous modeling efforts. This fact points out the need to refine the characteristics of the input parameters that are commonly used to drive the numerical models. We suggest that changing the altitude or latitudinal distribution of the vertical $\mathbf{E}\times\mathbf{B}$ drifts may produce wider or narrower and more or less pronounced anomaly crests. New modeling efforts are needed in order to prove this point.

The presence of asymmetric anomaly peaks and the occurrence of a rapid decay of a larger crest have been interpreted as an indication of the effect of a persistent transequatorial neutral wind blowing the *F* region density from one hemisphere toward the opposite, creating a larger TEC crest in the downwind hemisphere. If the transequatorial wind persists for several hours after sunset, a significant lowering of the *F* layer may occur, which initiates a rapid recombination of the *F* layer. This argument was used by *Maruyama and Matuura* [1984] to suggest that the transequatorial wind could be a stabilizing mechanism due to the lowering of the *F* region in the upwind hemisphere. We have not seen such an effect, but at the same time we acknowledge the lack of completeness in the Northern Hemisphere portion of our TEC distributions.

We have been able to parameterize the TEC distributions using the location and amplitude of the anomaly peaks as controlling parameters. However, we found that these parameters could not be used unequivocally to define the onset of ESF. In contrast to this, time difference profiles of the distributions at 1800 and 2000 LT had a far superior correlation with the occurrence of ESF. We suggest that carrying out a real-time tracking of the variability of the time difference profiles may help us to get closer to a forecasting capability of the occurrence of ESF. However, several other steps have to be carried out concurrently with making the pseudorange and phase data available on real time. One consists of assessing how much earlier before sunset is it possible to obtain a reliable estimate of the trend that the TEC profiles have at the crests and the trough. Another important one is determining whether all the scintillation events correspond to cases of well-elongated plasma plumes extending to the topside and to see if scintillation events with different characteristics (S4 and spectral slope) are accompanied by different types of TEC distributions. Finally, it is necessary to prove that only a partial pass of a GPS satellite can be used to obtain absolute values of TEC.

6. Conclusions

This investigation has led to the following insights:

1. The SCORE program was used to process daily RINEX files corresponding to all the days in 1998 when data were acquired by any of the six stations. The excellent agreement that we found in the TEC values measured at common boundaries during consecutive days and at adjacent stations reaffirms the merits of the processing technique that we used to obtain TEC values.

2. The TEC latitudinal distributions show the presence of two crests varying in location between 12° and 20° and a trough situated near the magnetic equator. The crests develop at local times when the vertical velocity is upward. This fact is in agreement with the role of the fountain effect as the generator of the equatorial anomaly. On a few days we observed, in the early evening, an increase of the TEC values at the trough. This fact suggests the appearance of a reverse fountain effect occurring right after sunset.

3. We determined the presence/absence of ESF (plumes) based on the RTI maps collected by the JULIA radar and records of scintillation from two stations spaced in latitude. One of the scintillation stations is located near the magnetic equator (Ancon), and the other one is located at −11° magnetic latitude (Antofagasta).

4. Close comparison between the appearance of ESF and the difference of TEC profiles obtained at 1800 and 2000 LT indicates that during the equinoxes and the December solstice, ESF develops on nights when there is a decrease of the TEC values at the trough and an augmentation of TEC at the crests.

5. The location and amplitude of the crests and trough and the integrated TEC value inside the southern anomaly have been used to parameterize the TEC distributions. We found that during the equinoxes the TEC value at the trough can be related to the ESF activity. When the trough TEC value is below 30 units, plumes were present most of the time, but for higher values the plumes were absent.

6. The presence of only one GPS receiver at latitudes north of Ancon limited the possibilities of resolving the northern crest in 1998. Nevertheless, a new GPS receiver has already been deployed at 3.8°S latitude (7.8° magnetic latitude) in February 2000, and four more will be placed in late 2000 and 2001. This will allow us to fully characterize the northern crest of the anomaly and to examine the effect of the meridional winds by looking at the asymmetry of the peaks.

Acknowledgments. The authors would like to thank G. Bishop of the Air Force Research Laboratory for allowing us to use the SCORE program, which was instrumental in the success of this study. M. Bevis and E. Kendrick of the University of Hawaii provided data from their Iquique and Copiapo stations; both stations are part of the South Andes Project (SAP). We are grateful to Su. Basu for her helpful comments and suggestions on the paper. We thank Jorge Espinoza and Ruben Villafani for their dedication to the smooth operation of the spaced receiver scintillation instrument at Ancon, Peru. One of the authors (C.E.V.) thanks R. F. Woodman and the personnel of the Jicamarca Radio Observatory for their hospitality during a six-month sabbatical visit in which part of this work was conducted. The work at Boston College was partially supported by NSF grants ATM-9714804 and ATM-9819912, and by Air Force Research Laboratory contract F19628-97-C-0094. The work at the Air Force Research Laboratory was partially supported by AFOSR task 231069 and 2311SDA4. The observatory of Ancon is operated by the Geophysical Institute of Peru, Ministry of Education. The Jicamarca Radio Observatory is operated by the Geophysical Institute of Peru, Ministry of Education, with support from the National Science Foundation Cooperative Agreements ATM-9022717 and ATM-9408441 to Cornell University.
Janet G. Luhmann thanks Graham J. Bailey and another referee for their assistance in evaluating this paper.

References

Aggson, T. L., N. C. Maynard, W. B. Hanson, and J. L. Saba, Electric field observations of equatorial bubbles, *J. Geophys. Res.*, *97*, 2997, 1992.

Balan, N., and G. J. Bailey, Equatorial plasma fountain and its effects: Possibility of an additional layer, *J. Geophys. Res.*, *100*, 21,421, 1995.

Basu, Su, and S. Basu, Equatorial scintillations: Advances since ISEA-6, *J. Atmos. Terr. Phys.*, *47*, 753, 1985.

Basu, S., et al., Scintillations, plasma drifts, and neutral winds in the equatorial ionosphere after sunset, *J. Geophys. Res.*, *101*, 26795, 1996.

Bishop, G. J., A. Mazzella, E. Holland, and S. Rao, Algorithms that use the ionosphere to control GPS errors, paper presented at *Position Location and Navigation Symposium (PLANS)*, Inst. of Electr. and Electr. Eng. Piscataway, N. J., 1996.

Bishop, G. J., A. J. Mazzella, S. Rao, A. Batchelor, P. Fleming, N. Lunt, and L. Kersley, Validations of the SCORE process, paper presented at *ION National Technology Meeting*, Inst. of Navig., Alexandria, Va., 1997.

Booker, H. G., and H. W. Wells, Scattering of radio waves by the *F* region of the ionosphere, *J. Geophys. Res.*, *43*, 249, 1938.

Crain, D.J., R.A. Heelis, G.J. Bailey, and A.D. Richmond, low-latitude plasma drifts from a simulation of the global atmospheric dynamo, *J. Geophys. Res.*, *98*, 6039, 1993.

Doherty, P.H., P. J. Gendron, R. Loh, and D. N. Anderson, "The spatial and temporal variations in ionospheric range delay", paper presented at *the Institute of Navigation GPS-97*, Sept. 1997.

Farley, D. T., and D. L. Hysell, Radar measurements of very small aspect angles in the equatorial ionosphere, *J. Geophys. Res.*, *101*, 5177, 1996.

Farley, D. T., B. B. Balsley, R. F. Woodman, and J. P. McClure, Equatorial spread *F*: Implications of VHF radar observations, *J. Geophys. Res.*, *75*, 7199, 1970.

Farley, D.T., E. Bonnelli, B.G. Fejer, and M.F. Larsen, The prereversal enhancement of the zonal electric field in the equatorial ionosphere, *J. Geophys. Res.*, *91*, 13,723, 1986.

Fejer, B.G., E.R. de Paula, S.A. Gonzalez, and R.F. Woodman, Average vertical and zonal *F* region plasma drifts over Jicamarca, *J. Geophys. Res.*, *96*, 13,901, 1991.

Fejer, B.G., L. Scherliess, and E.R. de Paula, Effects of the vertical plasma drift velocity on the generation and evolution of equatorial spread F, *J. Geophys. Res.*, *104*, 19,859, 1999.

Groves, K. M., et al., Equatorial scintillation and systems support, *Radio Sci.*, *32*, 2947, 1997.

Hanson, W. B., and R. J. Moffett, Ionization transport effects in the equatorial *F* region *J. Geophys. Res.*, *71*, 5559, 1966.

Hanson, W. B., S. Sanatani, and T. N. L. Patterson, Influence of the *E* region dynamo on equatorial spread *F*, *J. Geophys. Res.*, *88*, 3169, 1983.

Hanson, W.B., B.L. Cragin, and A. Dennis, The effect of vertical drift on the equatorial *F*-region stability, *J. Atmos. Terr. Phys.*, *48*, 205, 1986.

Hanson, W. B., W. R. Coley, R. A. Heelis, and A. Urquhart, Fast equatorial bubbles, *J. Geophys. Res.*, *102*, 2039, 1997.

Huang, C. Y., W. J. Burke, J. S. Machuzak, L. C. Gentile, and P. J. Sultan, DMSP observations of equatorial plasma bubbles in the topside ionosphere near solar maximum, *J. Geophys. Res.*, *106*, 8131, 2001.

Hysell, D. L., and J. D. Burcham, JULIA radar studies of equatorial spread F, *J. Geophys. Res.*, **103**, 29155, 1998.

Hysell, D. L., M.C. Kelley, W. E. Swartz, and R.F. Woodman, Seeding and layering of equatorial spread *F* by gravity waves, *J. Geophys. Res.*, *95*, 17,253, 1990.

Jayanchandran, B., N. Balan, P. B. Rao, J. H. Sastri, and G. J. Bailey, HF Doppler and ionosonde observations on the onset conditions of equatorial spread *F*, *J. Geophys. Res.*, *98*, 13,741, 1993.

Kelley, M. C., G. Haerendel, H. Kappler, A. Valenzuela, B. B. Balsley, D. A. Carter, W. L. Ecklund, C. W. Carlson, B. Hausler, and R. Torbert, Evidence for a Rayleigh-Taylor type instability and upwelling of depleted density regions during equatorial spread *F*, *Geophys. Res. Lett.*, *3*, 448, 1976.

Kelley, M. C., M. F. Larsen, and C. LaHoz, Gravity wave interaction of equatorial spread *F*: A case study, *J. Geophys. Res.*, *86*, 9087, 1981.

Kelley, M. C., et al., The Condor equatorial spread *F* campaign: Overview and results of the large scale measurements, *J. Geophys. Res.*, *91*, 5487, 1986.

Kelley, M. C., D. Kotsikopoulos, T. Beach, and D. L. Hysell, Simultaneous global positioning system and radar observations of equatorial spread *F* at Kwajalein, *J. Geophys. Res.*, *101*, 2333, 1996.

Kudeki, E., B. G. Fejer, D. T. Farley, and H. M. Ierkic, Interferometer studies of equatorial *F* region irregularities and drifts, *Geophys. Res. Lett.*, *8*, 377, 1981.

Lunt, N., L. Kersley, G. J. Bishop, and A. J. Mazzella Jr., The contribution of the protonosphere to GPS total electron content: Experimental measurements, *Radio Sci.*, *34*, 1273, 1999a.

Lunt, N., L. Kersley, G. J. Bishop, A. J. Mazzella Jr., and G. J. Bailey, The protonospheric contribution to GPS total electron content: Two-station measurements, *Radio Sci.*, *34*, 1281, 1999b.

Maruyama, T., Modeling study of equatorial ionospheric height and spread *F* occurrence, *J. Geophys. Res.*, *101*, 5157, 1996.

Maruyama, T., and N. Matuura, Longitudinal variability of annual changes in activity of equatorial spread *F* and plasma bubbles, *J. Geophys. Res.*, *89*, 10,903, 1984.

McClure, J.P., W.B. Hanson, and J.H. Hoffman, Plasma bubbles and irregularities in the equatorial ionosphere, *J. Geophys. Res.*, *82*, 2650, 1977.

Mendillo, M., J. Baumgardner, X. Pi, P.J. Sultan, and R. Tsunoda, Onset conditions for equatorial spread *F*, *J. Geophys. Res.*, *97*, 13,865, 1992.

Ossakow, S. L., S. T. Zalesak, B. E. McDonald, and P. K. Chaturvedi, Nonlinear equatorial spread-*F*: Dependence on altitude of the *F* peak and bottomside background electron density gradient scale length, *J. Geophys. Res.*, *84*, 17, 1979.

Pi, X., A. J. Mannucci, U. J. Lindqwister, and C. M. Ho, Monitoring of global ionospheric irregularities using a worldwide GPS network, *Geophys, Res. Lett.*, *24*, 2283, 1997.

Raghavarao, R., M. Nageshwararao, J. Hanumath Sastri, G. D. Vyas, and M. Sriramarao, Role of equatorial ionization anomaly in the initiation of equatorial spread-*F*, *J. Geophys. Res.*, *93*, 5959, 1988.

Sastri, J. H., M. A. Abdu, I. S. Batista, and J. H. A. Sobral, Onset conditions of equatorial (range) spread *F* at Fortaleza, Brazil, during the June solstice, *J. Geophys. Res.*, *102*, 24,013, 1997.

Sridharan, R., R. Sekar, and S. Gurubaran, Two-dimensional high-resolution imaging of the equatorial plasma fountain, *J. Atmos. Terr. Phys.*, *55*, 1661, 1993.

Sridharan, R., D. PallamRaju, R. Raghavarao, and P. V. S. Ramarao, Precursor to equatorial spread-*F* in OI 630.0 nm dayglow, *Geophys. Res. Lett.*, *21*, 2797, 1994.

Sultan, P. J., and F. I. Rich, Observations and modeling of the seasonal and longitudinal occurrence pattern of equatorial spread-*F*, paper presented at Chapman Conference on Space Weather: Progress and Challenges in Research and Applications, AGU, Clearwater, Fa., March 2000.

Tsunoda, R. T., On the spatial relationship of 1-m equatorial spread *F* irregularities and plasma bubbles, *J. Geophys. Res.*, *85*, 185, 1980.

Tsunoda, R. T., Control of the seasonal and longitudinal occurrence of equatorial scintillations by the longitudinal gradient in the integrated *E* region Pedersen conductivity, *J. Geophys. Res.*, *90*, 447, 1985.

Valladares, C.E., W.B. Hanson, J.P. McClure, and B.L. Cragin, Bottomside sinusoidal irregularities in the equatorial F-region, *J. Geophys. Res.*, *88*, 8025, 1983.

Vladimer, J. A., P. Jastrzebski, M. C. Lee, P. H. Doherty, D. T. Decker, and D. N. Anderson, Longitude structure of ionospheric total electron content at low latitudes measured by the TOPEX/Poseidon satellite, *Radio Sci.*, *34*, 1239, 1999.

Walker, G. O., J. H. K. Ma, and E. Golton, The equatorial ionospheric anomaly in electron content from solar minimum for South East Asia, *Ann. Geophys.*, *12*, 195, 1994.

Weber, E. J., et al., Equatorial plasma depletion precursor signatures and onset observed at 11° south of the magnetic equator, *J. Geophys. Res.*, *101*, 26,829, 1996.

Woodman, R.F., Vertical drift velocities and east-west electric fields at the magnetic equator, *J. Geophys. Res.*, *75*, 6249, 1970.

Woodman, R.F., and C. LaHoz, Radar observations of *F* region equatorial irregularities, *J. Geophys. Res.*, *81*, 5447, 1976.

Zalesak, S. T., and S. L. Ossakow, Nonlinear equatorial spread *F*: Spatially large bubbles resulting from large horizontal scale initial perturbations, *J. Geophys. Res.*, *85*, 2131, 1980.

S. Basu and K. Groves, Air Force Research Laboratory, Hanscom AFB, MA 01731.

M. P. Hagan, R. E. Sheehan, and C. E. Valladares, Institute for Scientific Research, Boston College, 140 Commonwealth Ave., Chesnut Hill, MA 02467. (valladar@bc.edu).

D. Hysell, Department of Physics and Astronomy, Clemson University, Clemson, SC 29634.

A. J. Mazzella Jr., Northwest Research Associates, Bellevue, WA 98809.

(Received November 15, 2000; revised March 21, 2001; accepted March 23, 2001.)